Composites Part B 108 (2017) 279–290

Contents lists available at ScienceDirect

Composites Part B

journal homepage: www.elsevier.com/locate/compositesb

Thermoelastic buckling of FGM conical shells under non-linear temperature rise in the framework of the shear deformation theory

A.H. Sofiyev [a, *], Z. Zerin [b], N. Kuruoglu [c]

[a] Department of Civil Engineering, Faculty of Engineering of Suleyman Demirel University, Isparta, Turkey
[b] Department of Civil Engineering, Faculty of Engineering of Ondokuz Mayis University University, Samsun, Turkey
[c] Department of Civil Engineering, Faculty of Engineering and Architecture of Istanbul Gelisim University, Istanbul, Turkey

ARTICLE INFO

Article history:
Received 6 August 2016
Accepted 29 September 2016
Available online 3 October 2016

Keywords:
Thermomechanical
Buckling
Analytical modelling
Numerical analysis

ABSTRACT

In this study, the thermoelastic buckling of functionally graded material (FGM) conical shells under non-linear temperature rise across the thickness in the framework of the shear deformation theory (SDT) is investigated. To the derivation of basic equations is used modified Donnell-type shell theory. The Galerkin method is used to obtain the formula for non-linear buckling temperature difference of freely supported FGM truncated conical shell in the framework of the SDT. By changing the properties of FGMs and volume fraction index, the effect of transverse shear deformations on the non-linear buckling temperature difference is evaluated by comparing with the results of the classical shell theory (CST). Meanwhile, the effect of geometric parameters on the non-linear buckling temperature difference of the shear deformable FGM conical shells is discussed in detail.

1. Introduction

In modern industries the use of new composite materials in conical shells are increased because of their ability to control stresses caused by thermal and mechanical loads. Functionally graded materials (FGMs) are new kind of composite materials, in which the elastic and thermal properties change from one surface to the other, gradually and continuously. The material is constructed by smoothly changing the volume fraction of its constituent materials. Typically, FGMs are made from a mixture of ceramic and metal. Since the ceramics has a good heat resistance and metal has high strength, the FGMs can operate at high temperatures difference area. With the excellent performance in ultrahigh temperature circumstance, FGMs are generally designed as thermal barriers for spacecraft and nuclear reactor, etc. [1–5].

With the increasing applications of FGMs in modern technology, thermo-mechanical analysis of FG structures began to attract a widespread attention. Thus, many studies on the thermo-mechanical buckling analysis of FG shells have been published in the literature that most of these studies relating to FG cylindrical shells. Notable among them are due to Shahsiah and Eslami [6] studied functionally graded cylindrical shell thermal instability based on improved Donnell equations. Na and Kim [7] presented three-dimensional thermal buckling analysis of FGMs by using an 18-node solid element to analyze more accurately the variation of material properties and temperature field in the thickness direction. Wu et al. [8] discussed the problems of thermal buckling in axial direction of cylindrical shells made of FGMs based on the classical Donnell's shell theory. Shariyat [9] presented the dynamic buckling of a pre-stressed, suddenly heated imperfect FGM cylindrical shell and dynamic buckling of a mechanically loaded imperfect FGM cylindrical shell in thermal environment, with temperature-dependent properties using modified Budiansky criterion proposed by the author. Cavalcante et al. [10] studied transient finite-volume analysis of a graded cylindrical shell subjected to transient thermal cyclic loading, which simulates a thermal shock durability test, using the parametric finite-volume theory for functionally graded materials. Wosu et al. [11] studied hygro-thermal effects on the dynamic compressive properties of graphite/epoxy composite material. Heydarpour et al. [12] investigated the thermoelastic behavior of rotating laminated functionally graded (FG) cylindrical shells in thermal environment using the differential quadrature method (DQM) and developed an accurate and efficient solution procedure based on the elasticity theory. Bagherizadeh et al. [13] presented thermal buckling of functionally graded material cylindrical shells on elastic foundation. Shen [14] investigated

* Corresponding author.
E-mail address: abdullahavey@sdu.edu.tr (A.H. Sofiyev).

http://dx.doi.org/10.1016/j.compositesb.2016.09.102
1359-8368/

thermal buckling and postbuckling behavior of functionally graded carbon nanotube-reinforced composite cylindrical shells subjected to a uniform temperature rise based on the SDT. Shariyat and Asgari [15] analyzed nonlinear thermal buckling and postbuckling analyses of imperfect, variable thickness cylindrical shells made of bidirectional functionally graded materials undergoing uniform temperature rises are accomplished for the first time, employing a third-order shear-deformation theory, von Karman-type kinematic nonlinearity, nonlinear finite element method and modified Budiansky's criterion. Sheng and Wang [16] presented an analytical method and a new simplifying model of FG cylindrical shells based on Hamilton's principle, Von Kármán non-linear theory and the first-order shear deformation theory, and subjected to thermal and axial loads using a series expansion of linear modes and a multi-term Galerkin's method. Dai et al. [17] studied buckling analysis for a ring-stiffened FGM cylindrical shell under hydrostatic pressure and thermal loads. Mansouri and Shariyat [18] investigated biaxial thermo-mechanical buckling of orthotropic auxetic FGM plates with temperature and moisture dependent material properties. Sun et al. [19] investigated buckling analysis for shear deformable FGM cylindrical shells under axial compression and thermal loads based on the Reddy's high-order shear deformation theory. Sun et al. [20] presented an accurate buckling analysis for piezoelectric fiber-reinforced composite (PFRC) cylindrical shells subjected to combined loads comprising compression, external voltage and thermal load, based on Reddy's higher-order shear deformation theory. Alibeigloo [21] investigated thermoelastic analysis of FG carbon nanotube reinforced composite cylindrical panel attached to thin piezoelectric layers subjected to thermal, mechanical loads and electric field using the Fourier series. Jabbari et al. [22] developed the general solution of steady-state 1D radially symmetric mechanical and thermal stresses and electrical and mechanical displacements for a hollow thick cylinder made of fluid-saturated functionally graded poro piezoelectric materials (FGPPMs) using complex Fourier series. Khazaeinejad and Usmani [23] developed a theoretical model for the geometrically nonlinear analysis of shallow shells with single and double curvatures and subjected to thermo-mechanical loadings.

The thermal stability problems associated with the FGM conical shells have been less studied compared with the other FGM structural elements. Among them, the linear thermal buckling of functionally graded truncated conical shells using the semi-analytical finite element method within the FSDT was analyzed by Bhangale et al. [24]. The thermo-elastic stability of FGM truncated conical shells in the framework of the CST was studied by Sofiyev [25]. Thermal and mechanical instability of truncated conical shells made of FGM within the FSDT using Sanders nonlinear kinematics equations were investigated by Naj et al. [26]. The linear thermal buckling analysis of truncated hybrid FGM conical shells based on the CST using Sanders nonlinear kinematics equations was analyzed by Torabi et al. [27]. The thermal stability of temperature-dependent FGM conical shells within the CST using the Fourier-DQM method was solved by Akbari et al. [28] analytically. Thermal buckling of temperature dependent FG-CNT reinforced composite conical shells within the FSDT employing discrete singular convolution method was studied by Mirzaei and Kiani [29]. Nonlinear thermal stability of eccentrically stiffened functionally graded truncated conical shells surrounded on elastic foundation within the CST was investigated by Duc and Pham [30]. In recent years, various shear deformation theory have received more attention in the study of advanced composite structures [31–36].

The above literature survey reveals that the thermal buckling of FGM conical shells based on the SDT is restricted in number. Thermoelastic stability of freely supported FGM conical shells under uniform and linear temperature rises within the SDT was investigated by Sofiyev [37]. In the present study, an attempt is made to address the closed form solution of thermal buckling of FGM conical shells subjected to the non-linear temperature rise across the thickness. The material properties of the constituents are graded in the thickness direction according to a power-law distribution. The basic equations of FGM truncated conical shells under non-linear temperature rise within the SDT are derived using modified Donnell type shell theory. Solving the basic equations using Galerkin method the expression for the critical temperature difference of FGM conical shells subjected to the non-linearly distributed temperature across the thickness based on the SDT is obtained. The appropriate formulas for FGM cylindrical shells based on the SDT are found as a special case.

2. Theoretical development

Consider an FGM truncated conical shell as presented in Fig. 1. The geometric parameters are defined as the length L, the semi-vertex angle γ , the small and large ends radii R_1 and R_2 and the thickness h. A set of curvilinear coordinates (z, θ, S) is located on the reference surface, which the z-axis is always normal to the moving S axis and points inwards, θ axis is in the direction perpendicular to the (S, z) surface. S_1 and S_2 are the distances from the vertex to the small and large bases, respectively.

Using the Voigt model as the rule of the mixture approximation [2,39], and a simple power law distribution for volume fraction such as [38,39].

$$V_i = (Z + 0.5)^k, \quad V_i + V_o = 1 \tag{1}$$

where $Z=z/h$ denotes normalized thickness coordinate, the subscripts "i" and "o" represent the properties of inner and outer constituents, respectively, and volume fraction index k ($k\geq 0$) dictates the material variation profile through the FGM shell thickness.

The property variation of an FGM conical shell, such as Young's modulus $E_f(Z)$, thermal conductivity $K_f(Z)$ and thermal expansion coefficient $\alpha_f(Z)$ is given by Refs. [37–39].

$$E_f(Z) = E_oV_o + E_iV_i, \quad K_f(Z) = K_oV_o + K_iV_i, \quad \alpha_f(Z) = \alpha_oV_o + \alpha_iV_i \tag{2}$$

The Poisson' s ratio is assumed to be a constant, i.e., $\nu_f(Z)=\nu$.

In this study, two different types of FGM conical shells are involved: Type A conical shell (FGM-A) the outer surface is metal-rich and the inner surface is ceramic-rich. Type B conical shell (FGM-B) will reverse compositional distribution.

From Eqs. (1)–(3), one has

$$E_f(Z) = (E_i - E_o)(Z + 0.5)^k + E_o, \quad K_f(Z) = (K_i - K_o)(Z + 0.5)^k + K_o$$
$$\alpha_f(Z) = (\alpha_i - \alpha_o)(Z + 0.5)^k + \alpha_o, \quad \nu_f(Z) = \nu = \text{const} \tag{3}$$

FGM's are designed in order to resist high temperature rise by ceramic, so the temperature change will be quite different at the two sides of FGM conical shells. The one-dimensional heat conduction equation in the absence of heat generation for FGM conical shells becomes [39].

$$\frac{d}{d\bar{Z}}\left[K_f(Z)\frac{dT}{d\bar{Z}}\right] = 0 \tag{4}$$

where $K_f(Z)$ is the coefficient of the thermal conduction. The boundary conditions for the temperature profile associated with the above equation are

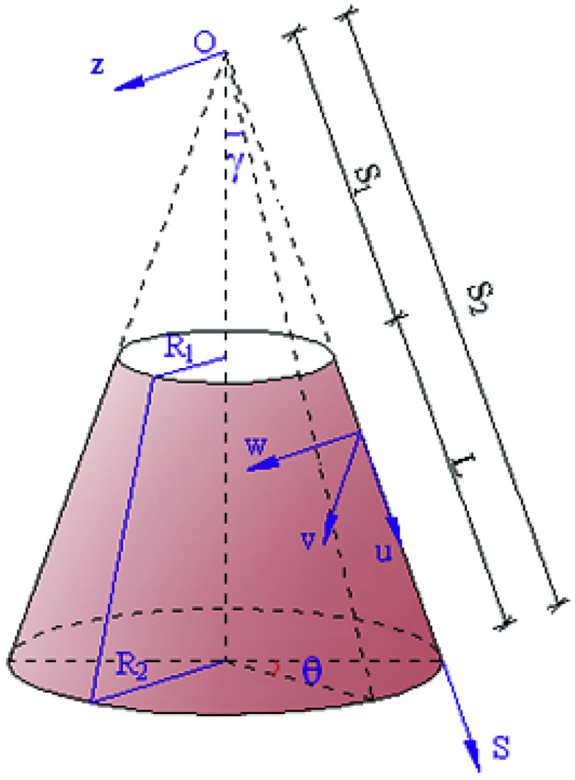

Fig. 1. FGM truncated conical shell and coordinate system.

$$\begin{aligned} T &= T_o \quad at \quad z = -h/2, \\ T &= T_i \quad at \quad z = +h/2 \end{aligned} \tag{5}$$

Similar to the elasticity and thermal expansion properties, we assume that the thermal conductive coefficient is also a power form function as

$$K_f(Z) = (K_i - K_o)(Z + 0.5)^k + K_o \tag{6}$$

The solution of Eq. (4) is obtained by means of polynomial series. Taking the first seven terms of the series, the solution for temperature distribution across the shell thickness becomes

$$T(Z) = T_o + \Delta T \Lambda(Z) \tag{7}$$

where $\Delta T = T_i - T_o$ is defined as the temperature difference between outer and inner metal-rich surfaces of the FGM conical shell and the following definition applies:

$$\begin{aligned} \Lambda(Z) = \frac{1}{\Pi}\Bigg[& Z + 0.5 - \frac{K_0}{k+1}(Z+0.5)^{k+1} + \frac{K_0^2}{2k+1}(Z+0.5)^{2k+1} \\ & - \frac{K_0^3}{3k+1}(Z+0.5)^{3k+1} + \frac{K_0^4}{4k+1}(Z+0.5)^{4k+1} \\ & - \frac{K_0^5}{5k+1}(Z+0.5)^{5k+1}\Bigg] \end{aligned} \tag{8}$$

in which the following definitions apply:

$$\Pi = 1 - \frac{K_0}{k+1} + \frac{K_0^2}{2k+1} - \frac{K_0^3}{3k+1} + \frac{K_0^4}{4k+1} - \frac{K_0^5}{5k+1}, \quad K_0 = \frac{K_i}{K_o} - 1 \tag{9}$$

3. Basic equations

To capture the through the thickness shear deformations effects, the FSDT is used to formulate the governing equations of the FGM conical shells. According to first order shear deformation shell theory, components of the displacement on a generic point of the FGM conical shell may be represented according to the mid-surface characteristics such that [40].

$$\begin{aligned} u_1(x,\theta,z) &= u(x,\theta) + z\eta_1(x,\theta), \quad v_1(x,\theta,z) \\ &= v(x,\theta) + z\eta_2(x,\theta), \quad w_1(x,\theta,z) = w(x,\theta) \end{aligned} \tag{10}$$

In the above equation, $u(x,\theta)$, $v(x,\theta)$ and $w(x,\theta)$ are the meridional, circumferential and radial direction displacements of the mid-surface, respectively, and $x = ln(S/S_2)$ is a variable. Besides, $\eta_2(x,\theta)$ and $\eta_1(x,\theta)$ are the transverse normal rotations about S and θ axes, respectively.

The constitutive relations for FGM conical shells by considering the temperature effect becomes

$$\begin{bmatrix} \sigma_S \\ \sigma_\theta \\ \sigma_{S\theta} \\ \sigma_{Sz} \\ \sigma_{\theta z} \end{bmatrix} = \begin{bmatrix} K_{11}(Z) & K_{12}(Z) & 0 & 0 & 0 \\ K_{12}(Z) & K_{11}(Z) & 0 & 0 & 0 \\ 0 & 0 & K_{33}(Z) & 0 & 0 \\ 0 & 0 & 0 & K_{33}(Z) & 0 \\ 0 & 0 & 0 & 0 & K_{33}(Z) \end{bmatrix} \begin{bmatrix} \varepsilon_S \\ \varepsilon_\theta \\ \gamma_{S\theta} \\ \gamma_{Sz} \\ \gamma_{\theta z} \end{bmatrix} + \begin{bmatrix} \sigma_T \\ \sigma_T \\ 0 \\ 0 \\ 0 \end{bmatrix} \tag{11}$$

where σ_S, σ_θ, $\sigma_{S\theta}$, σ_{Sz}, $\sigma_{\theta z}$ indicate the stresses and ε_S, ε_θ, $\gamma_{S\theta}$,γ_{Sz},$\gamma_{\theta z}$ indicate the strains in the FGM conical shell, K_{ij}(i, j=1, 2, 3) are the FGM properties and are defined as:

$$\begin{aligned} K_{11}(Z) = \frac{E_f(Z)}{1-\nu^2}, \quad K_{12}(Z) = \frac{\nu E_f(Z)}{1-\nu^2}, \quad K_{33}(Z) = G_{12}(Z) = G_{13}(Z) \\ = G_{23}(Z) = \frac{E_f(Z)}{2(1+\nu)} \end{aligned} \tag{12}$$

In addition, the temperature stress,σ_T, is defined as

$$\sigma_T = -\frac{E_f(Z)\alpha_f(Z)T(Z)}{1-\nu} \tag{13}$$

Transverse shear stresses σ_{Sz} and $\sigma_{\theta z}$ for the FGM conical shell are expressed, as [37,40,42].

$$\sigma_{Sz} = \frac{df(z)}{dz}\eta_1(x,\varphi), \quad \sigma_{\theta z} = \frac{df(z)}{dz}\eta_2(x,\varphi) \tag{14}$$

where $\varphi = \theta \sin\gamma$ and $f(z)$, $(i=1, 2)$ represent the posteriori specified shape function which, determine the through-the-thickness distribution of the transverse shear stresses of the FG shell [31–37,42].

According to the FSDT and using Eqs. (10), (11) and (14), the components of strain field on an arbitrary point of the shell may be obtained in terms of those belong to the mid-surface of the FGM

conical shell and change of curvatures. Consequently, one may write [37]:

$$\varepsilon_S = \varepsilon_{0S} - \frac{z}{S_2^2 e^{2x}}\left(\frac{\partial^2 w}{\partial x^2} - \frac{\partial w}{\partial x}\right) + \frac{I(z)}{S_2 e^x}\frac{\partial \eta_1}{\partial x}$$
$$\varepsilon_\theta = \varepsilon_{0\theta} - \frac{z}{S_2^2 e^{2x}}\left(\frac{\partial^2 w}{\partial \varphi^2} + \frac{\partial w}{\partial x}\right) + \frac{I(z)}{S_2 e^x}\frac{\partial \eta_2}{\partial \varphi} \quad (15)$$
$$\gamma_{S\theta} = \gamma_{0S\theta} - \frac{2z}{S_2^2 e^{2x}}\left(\frac{\partial^2 w}{\partial x \partial \varphi} - \frac{\partial w}{\partial \varphi}\right) + \frac{I(z)}{S_2 e^x}\left(\frac{\partial \eta_1}{\partial \varphi} + \frac{\partial \eta_2}{\partial x}\right)$$

where ε_{0S} and $\varepsilon_{0\theta}$ are normal strains in the S and θ directions, $\gamma_{0S\theta}$ is the shear strain on the reference surface of FGM truncated conical shells and $I(z)$ is function including the shear stresses effects and given by

$$I(z) = \int_0^z \frac{df(z)}{dz}\frac{1}{K_{33}(Z)}dz \quad (16)$$

The resultant forces and moments per unit length based on the FSDT can be figured out by integrating Eq. (9) through the shell thickness as [38,40].

$$(n_S, n_\theta, n_{S\theta}, q_S, q_\theta) = \int_{-h/2}^{h/2} (\sigma_S, \sigma_\theta, \sigma_{S\theta}, \sigma_{Sz}, \sigma_{\theta z})dz$$
$$(m_S, m_\theta, m_{S\theta}) = \int_{-h/2}^{h/2} (\sigma_S, \sigma_\theta, \sigma_{S\theta})zdz \quad (17)$$

where $(n_S, n_\theta, n_{S\theta})$ and $(m_S, m_\theta, m_{S\theta})$ represent the in-plane meridional, circumferential and shearing forces and moments, and (q_S, q_θ) represent the shear forces.

Introducing Airy's stress function, Ψ, the membrane resultant forces can be expressed by Refs. [38–40].

$$n_S = \frac{h}{S_2^2 e^{2x}}\left(\frac{\partial^2 \Psi}{\partial \varphi^2} + \frac{\partial \Psi}{\partial x}\right), \quad n_\theta = \frac{h}{S_2^2 e^{2x}}\left(\frac{\partial^2 \Psi}{\partial x^2} - \frac{\partial \Psi}{\partial x}\right),$$
$$n_{S\theta} = \frac{h}{S_2^2 e^{2x}}\left(\frac{\partial \Psi}{\partial \varphi} - \frac{\partial^2 \Psi}{\partial x \partial \varphi}\right) \quad (18)$$

The membrane form of equilibrium equations, one gets

$$n_S^0 = -\Phi = -\int_{-h/2}^{h/2} E_f(Z)\alpha_f(Z)T(Z)dz, \quad n_\theta^0 = 0, \quad n_{S\theta}^0 = 0 \quad (19)$$

where n_S^0 is the pre buckling thermal force and Φ is a thermal parameter.

Substituting Eq. (15) into Eq. (11) and combining Eq. (17), the resultant moments and resultant forces can be re-arranged into the functions of a transverse displacement w, two rotations η_1 and η_2, and the Airy stress function Ψ. Meanwhile, considering Eqs. (14) and (17), the resultant shear forces can also be expressed by the basic variables. Introducing them into the stability and strain compatibility equations, the governing equations for the FGM conical shells can be given in the following form:

$$\begin{aligned} &L_{11}(\Psi) + L_{12}(w) + L_{13}(\eta_1) + L_{14}(\eta_2) = 0\\ &L_{21}(\Psi) + L_{22}(w) + L_{23}(\eta_1) + L_{24}(\eta_2) = 0\\ &L_{31}(\Psi) + L_{32}(w) + L_{33}(\eta_1) + L_{34}(\eta_2) = 0\\ &L_{41}(\Psi) + L_{42}(w) + L_{43}(\eta_1) + L_{44}(\eta_2) = 0 \end{aligned} \quad (20)$$

where $L_{ij}(i=1, 2, \ldots, 4)$ are differential operators and are given in Appendix A.

4. Solution procedure

The approximate solution for Eq. (20), satisfying the freely supported boundary conditions may be assumed as [40]:

$$\begin{aligned} \Psi(x,\varphi) &= C_\Psi S_2\, e^{(\lambda+1)x}\sin(\alpha x)\cos(\beta\varphi)\\ w(x,\varphi) &= C_w e^{\lambda x}\sin(\alpha x)\cos(\beta\varphi)\\ \eta_1(x,\varphi) &= C_{\eta_1} e^{\lambda x}\cos(\alpha x)\cos(\beta\varphi)\\ \eta_2(x,\varphi) &= C_{\eta_2} e^{\lambda x}\sin(\alpha x)\sin(\beta\varphi) \end{aligned} \quad (21)$$

where $\alpha = m\pi/x_0$, $\beta = n/\sin\gamma$, $x_0 = \ln S_1/S_2$, in which, m and n are the numbers of meridional half wave and circumferential wave, λ is an unknown parameter that will be determined from the minimum conditions of critical temperature differences and C_Ψ, C_w, $C_{\eta 1}$, $C_{\eta 2}$are unknown coefficients.

Substitute Eq. (21) into Eq. (20), and applying the Galerkin's method and then setting the determinant of coefficient matrix of resulting equations to zero, we have

$$p_{41}u_1 - \Phi p_T u_2 + p_{43}u_3 + p_{44}u_4 = 0 \quad (22)$$

where the following definitions apply:

$$\begin{aligned} u_1 &= -p_{12}p_{23}p_{34} + p_{12}p_{24}p_{33} - p_{22}p_{33}p_{14} + p_{22}p_{13}p_{34} - p_{32}p_{13}p_{24} + p_{32}p_{23}p_{14}\\ u_2 &= p_{11}p_{23}p_{34} - p_{11}p_{24}p_{33} + p_{21}p_{33}p_{14} - p_{21}p_{13}p_{34} + p_{31}p_{13}p_{24} - p_{31}p_{23}p_{14}\\ u_3 &= -p_{11}p_{22}p_{34} + p_{11}p_{24}p_{32} - p_{21}p_{32}p_{14} + p_{21}p_{12}p_{34} - p_{31}p_{12}p_{24} + p_{31}p_{22}p_{14}\\ u_4 &= p_{11}p_{22}p_{33} - p_{11}p_{23}p_{32} + p_{21}p_{32}p_{13} - p_{21}p_{12}p_{33} + p_{31}p_{12}p_{23} - p_{31}p_{22}p_{13} \end{aligned} \quad (23)$$

in which $p_{ij}(i, j=1, 2, \ldots, 4)$ are the parameters depending on the FGM conical shell characteristics within SDT, and p_T is the thermal parameter coefficient in which the details of the coefficients are found in Appendix B.

Substituting Eq. (7) into Eq. (19) yields

$$\Phi = PT_o + H_1\Delta T \quad (24)$$

where the following definitions apply:

$$P=h\int_{-0.5}^{0.5}\left[(E_i-E_o)(Z+0.5)^k+E_o\right]\left[(\alpha_i-\alpha_o)(Z+0.5)^k+\alpha_o\right]dZ$$
$$H_1=h\int_{-0.5}^{0.5}\left[(E_i-E_o)(Z+0.5)^k+E_o\right]\left[(\alpha_i-\alpha_o)(Z+0.5)^k+\alpha_o\right]\Lambda(Z)dZ \tag{25}$$

Substituting Eq. (24) into Eq. (22), we obtain an expression for the critical temperature difference of FGM conical shells based on the SDT, as the temperature change is a non-linear function as:

$$T_{NLcr}^{SDT}=-\Delta T_{cr}=\frac{1}{P-H_1}\frac{p_{41}u_1+p_{43}u_3+p_{44}u_4}{u_2p_T}-\frac{PT_i}{P-H_1} \tag{26}$$

If not take into account the transverse shear stresses, the expression (26) for the non-linear critical temperature difference based on the SDT are converted into the expressions for the non-linear critical temperature difference based on the CST, respectively, as follows:

$$T_{NLcr}^{CST}=-\Delta T_{cr}=\frac{1}{P-H_1}\frac{\overline{u}_1+\overline{u}_2}{\overline{u}_3\overline{p}_T}-\frac{PT_i}{P-H_1} \tag{27}$$

where $\overline{u}_j(j=1,2,3)$ and $\overline{p}_T$ are the parameters depending on the FGM conical shell characteristics based on the CST and the thermal parameter coefficient, respectively and are presented in Appendix C.

The minimum values of non-linear critical temperature differences based on SDT and CST are obtained by minimizing Eqs. (26) and (27), respectively, with respect to m, n and λ. The magnitudes of non-linear critical temperature differences for freely supported FGM truncated conical shells in the framework of STD and CST are found approximately at λ=2.1 and m=1.

From Eqs. (26) and (27), the non-linear critical temperature differences of ceramic-rich and metal-rich conical shells based on SDT and CST, respectively, are obtained, as the volume fraction index, k, is equal to zero and infinity.

From Eqs. (26) and (27), the formulas for the critical uniform temperature differences of FGM conical shells based on the SDT and CST, respectively, are obtained as:

$$T_{unicr}^{SDT}=\frac{p_{41}u_1+p_{43}u_3+p_{44}u_4}{Pu_2p_T} \tag{28}$$

and

$$T_{unicr}^{CST}=\frac{\overline{u}_1+\overline{u}_2}{P\overline{u}_3\overline{p}_T} \tag{29}$$

As the $\gamma\to0$, the critical uniform temperature differences of FGM cylindrical shells based on the SDT and CST are obtained, in a special case.

5. Result and discussion

5.1. Comparison studies

In order to verify the present method, comparison studies are carried out for the critical temperature difference with the given results in the literature. The firs comparison study is performed in Table 1 between the results of present study based on the CST and those reported by Wu et al. [8] and Torabi et al. [27]. As the $\gamma\to0$, from Eqs. (27) and (29), the critical non-linear and uniform temperature difference of FGM cylindrical shells based on the CST are obtained, respectively. In comparison the outer surface of FGM cylindrical shell is metal-rich, i.e., $E_f(Z)=(E_c-E_m)(Z+0.5)^k+E_m$, $\alpha_f(Z)=(\alpha_c-\alpha_m)(Z+0.5)^k+\alpha_m$ and $\nu_f(Z)$=ν=const. The material properties of the metal (Aluminum) and ceramic (Alumina) phases are taken to be $E_m=70GPa$, $\alpha_m=23\times10^{-6}(1/^\circ C)$, ν_m=0.3 and $E_c=380GPa$, $\alpha_c=7.4\times10^{-6}(1/^\circ C)$, ν_c=0.3. The data were taken from Refs. [8] and [27]. The FGM cylindrical shell characteristics are taken to be h=0.01m, L_1=1m and R=100h. It can be seen that the present results are in good agreement with results of Wu et al. [8] and Torabi et al. [27] for FGM cylindrical shells with different volume fraction index within the CST.

The next comparison study is performed in Table 2 between the results of this study based on the CST and those reported by Lu and Chang [42]. The conical shell is made from aluminum (Al) and the material properties are taken to be $E_m=70GPa$, $\alpha_m=23\times10^{-6}(1/K)$, ν_m=0.3. The results are presented for different values of height (H) of truncated conical shell that defined as H=R_1+R_2, and other geometrical parameters are taken to be γ=30° and h=0.01m. The data were taken from study of Lu and Chang [42]. To obtain the critical thermal load parameter (T_{cr}=$\alpha_m T$) of pure metal conical shells is used Eq. (29) at $k\to\infty$. The comparisons show that the present results very well agreed with the results of Lu and Chang [42]. The numbers in parentheses represent the buckling waves (m, n).

5.2. Thermal buckling analysis

In this study, two different types of FGM conical shells are considered: Type A conical shell (FGM A), the outer surface is metal-rich (Al) and the inner surface is ceramic-rich (Al_2O_3). Type B conical shell (FGM B) will reverse compositional distribution, i.e., the outer surface is ceramic-rich (Al_2O_3) and the inner surface is metal-rich (Al). The Young's modulus, coefficients of thermal expansion and thermal conductivity for the alumina (Al_2O_3) are $E_c=3.8\times10^{11}Pa, K_c=10.4W/mK, \alpha_c=7.4\times10^{-6}(1/^\circ C)$ and for the aluminum (Al) are taken to be $E_c=7\times10^{10}Pa, K_c=204W/mK$, $\alpha_c=23\times10^{-6}(1/^\circ C)$, respectively. The Poisson's ratio is taken to be constant, ν=ν_m=ν_c=0.3[8,27,38,39]. We assume that the temperature rise 5 °C in the outer surface of the FGM truncated conical shell. The materials are assumed to be perfectly elastic throughout the deformation. The truncated conical shell is subjected to non-linear temperature rise through the thickness. The shear stresses shape function is distributed the hyperbolic cosine (HYP) manner

Table 1
Comparison of critical uniform and non-linear temperature differences of FGM cylindrical shell with those of Wu et al. [8] and Torabi et al. [27].

k	Wu et al. [8]		Torabi et al. [27]	Present study	
	T_{unicr}^{CST}	T_{NLcr}^{CST}	T_{unicr}^{CST}	T_{unicr}^{CST}	T_{NLcr}^{CST}
0	817.88	1625.75	819.90	817.995(3,9)	1625.98(3,9)
1	414.13	664.3	416.60	414.13(4,9)	664.29(4,9)
2	364.8	614.19	365.80	364.81(5,7)	614.22 (5,7)
3	351.03	615.18	–	351.14(5,7)	615.36(5,7)

Table 2
Comparison of critical thermal load parameter of aluminum conical shells with the results of Lu and Chang [42].

H	$T_{cr} \times 10^3$(m,n)				
	200	300	400	500	600
Lu and Chang [42]	2.28	1.51	1.13	0.91	0.76
Present study	2.244(17,10)	1.493(17,15)	1.119(17,18)	0.896(19,20)	0.748(9,19)

through the conical shell thickness, i.e., $f(z) = h\sinh(z/h) - z\cosh(1/2)$ [31–36,41]. The volume fraction index are taken to be k=0; 0.5; 1.0; 2.0; 10 and ∞. To obtain the values of critical temperature differences T_{NLcr}(in C°) for non-linear temperature rise within SDT and CST are used Eqs. (26) and (27), respectively.

The non-linear critical temperature differences T_{NLcr}^{SDT} for FGM-A and FGM-B truncated conical shells in the framework of the SDT are compared with those of alumina (k=0) and aluminum (k=∞), FGM-A and FGM-B (k=0.5; 1.0; 2.0; 10) truncated conical shells within SDT as well as CST by estimating the percentage differences of values of non-linear critical temperature differences, respectively, as

$$\left(\frac{T_{NLcr}^{FGM} - T_{NLcr}^{H}}{T_{NLcr}^{H}}, \frac{T_{NLcr}^{SDT} - T_{NLcr}^{CST}}{T_{NLcr}^{CST}}\right) \times 100\% \tag{30}$$

The distribution of the values of T_{NLcr}^{SDT} and T_{NLcr}^{CST} (in C°) for alumina, aluminum, FGM-A and FGM-B truncated conical shells versus the semi-vertex-angle, γ, are presented in Table 3. Here, the volume fraction index is taken to be k=0.5; 1.0; 2.0; 10 andγ=0° represents the values of non-linear critical temperature differences of cylindrical shells. The conical shell characteristics are taken to be R_1=25h and R_1=5L. The values of T_{NLcr}^{SDT} and T_{NLcr}^{CST} of alumina, aluminum, FGM-A and FGM-B truncated conical shells decrease with the increasing of the semi-vertex-angle, γ. It is obvious that the magnitudes of T_{NLcr}^{SDT} for FGM-A conical shells higher than the T_{NLcr}^{SDT} of FGM-B conical shells for all semi-vertex-angle, γ . Furthermore, the magnitudes of T_{NLcr}^{SDT} and T_{NLcr}^{CST} for cylindrical shells higher than the T_{NLcr}^{SDT} and T_{NLcr}^{CST} for conical shells for all semi-vertex-angle, γ . The influences of shear stresses on the non-linear critical temperature differences decrease with the increasing of the semi-vertex-angle, γ. For instance; the influences of shear stresses on the values of non-linear critical temperature differences for FGM-A truncated conical shells decrease; from 7.98% to 7.37%, from 7.8% to 7.2%, from 8.75% to 8.24% and from 12.84% to 12.42%, while these influences for FGM-B truncated conical shells decrease; from 8.64% to 8.09%, from 7.8% to 7.2%, from 7.22% to 6.6% and from 7.82% to 7.2% for k=0.5; 1.0; 2.0; 10, respectively, as the semi-vertex-angle, γ, increases from 15° to 60°. The influence of shear stresses on the values of non-linear critical temperature differences for FGM-A truncated conical shells is higher than the FGM-B conical shells, as $k\leq1$, whereas, this influence is lower as k>1. It can be seen that the shear stresses effects on the non-linear critical temperature differences decrease, as the volume fraction index increases from 0.5 to 1, whereas, these influences increase, when the volume fraction index is higher one.

Comparing the values of non-linear critical temperature differences of FGM-A and FGM-B truncated conical shells with the alumina conical shell, the influences of FGM-A and FGM-B profiles on the values of T_{NLcr}^{SDT} and T_{NLcr}^{CST} nearly remain constant, while the influences of FGM-A conical shells decrease, whereas, the influences of FGM-B conical shells increase with the increasing of the semi-vertex angle, γ for k = 0.5; 1.0; 2.0. Table 3 reveals that the

Table 3
The distribution of the values of T_{NLcr}^{SDT} and T_{NLcr}^{CST} (in $^{\circ}C$) for alumina, aluminum, FGM-A and FGM-B truncated conical shells versus the semi-vertex-angle, γ.

	$T_{NLcr}^{SDT}(^{\circ}C)$ (m,n)					
		FGM-A				
γ	Alumina	k = 0.5	k = 1	k = 2	k = 10	Aluminum
0°	9927.94(1,1)	4640.60 (1,1)	3857.45(1.1)	3552.24(1,1)	3995.35(1,1)	3187.43(1,1)
15°	9803.08(1,1)	4576.26(1,1)	3811.03(1,1)	3509.49(1,1)	3958.76(1,1)	3147.25(1,1)
30°	9581.33(1,1)	4462.70(1,1)	3711.80(1,1)	3418.24(1,1)	3877.19(1,1)	3075.91(1,1)
45°	9315.80(1,1)	4326.68(1,1)	3592.94(1,1)	3308.96(1,1)	3779.85(1,1)	2990.47(1,1)
60°	9067.346(1,1)	4199.284(1,1)	3481.565(1,1)	3206.584(1,1)	3688.783(1,1)	2910.54(1,1)
γ	Alumina	FGM-B				Aluminum
0°	9927.94(1,1)	2516.16(1,2)	2659.16(1,1)	3032.36(1,1)	4135.20(1,1)	3187.43(1,1)
15°	9803.08(1,1)	2437.17(1,1)	2620.95(1,1)	2988.12(1,1)	4078.78(1,1)	3147.25(1,1)
30°	9581.33(1,1)	2416.51(1,2)	2552.72(1,1)	2909.07(1,1)	3978.18(1,1)	3075.91(1,1)
45°	9315.80(1,1)	2304.19 (1,1)	2470.89(1,1)	2814.23(1,1)	3857.58(1,1)	2990.47(1,1)
60°	9067.346(1,1)	2236.35(1,1)	2394.30(1,1)	2725.44(1,1)	3744.69(1,1)	2910.54(1,1)
	$T_{NLcr}^{CST}(^{\circ}C)$ (m,n)					
		FGM-A				
γ	Alumina	k = 0.5	k = 1	k = 2	k = 10	Aluminum
0°	10926.6 (1,1)	5043.02(1,1)	4193.78(1,1)	3902.16(1,1)	4594.073(1,1)	3508.72(1,1)
15°	10787.6(1,1)	4972.96(1,1)	4132.94(1,1)	3846.10(1,1)	4541.866(1,1)	3464.03(1,1)
30°	10526.8(1,1)	4841.60(1,1)	4019.02(1,1)	3741.09(1,1)	4443.288(1,1)	3380.09(1,1)
45°	10210.5(1,1)	4682.60(1,1)	3881.16(1,1)	3613.99(1,1)	4323.844(1,1)	3278.33(1,1)
60°	9913.9(1,1)	4533.38(1,1)	3751.77(1,1)	3494.71(1,1)	4211.766(1,1)	3182.91(1,1)
γ	Alumina	FGM-B				Aluminum
0°	10926.6 (1,1)	2756.93(1,2)	2884.19(1,1)	3268.96(1,1)	4486.87(1,1)	3508.72(1,1)
15°	10787.6(1,1)	2667.76(1,1)	2842.31(1,1)	3220.58 (1,1)	4424.72(1,1)	3464.03(1,1)
30°	10526.8(1,1)	2646.36 (1,2)	2764.00(1,1)	3130.16(1,1)	4308.33 (1,1)	3380.09(1,1)
45°	10210.5(1,1)	2512.81(1,1)	2669.12(1,1)	3020.62(1,1)	4167.29(1,1)	3278.33(1,1)
60°	9913.9(1,1)	2433.20(1,1)	2580.14(1,1)	2917.89(1,1)	4035.02(1,1)	3182.91(1,1)

greatest effect of compositional profiles (75%) occurs in the FGM-B conical shells, when compared with an alumina conical shell for k=0.5, whereas, the lowest effect of compositional profiles (5%) occurs in the conical shell made of FGM-B also, if it compared with an aluminum conical shell for k=2.

The distribution of the values of non-linear critical temperature differences, T_{NLcr}^{SDT} and T_{NLcr}^{CST} (in C°) versus theL/R_1, for k=0.5; 1.0; 2.0; 10 are demonstrated in Figs. 2 and 3 in which the truncated conical shells characteristics are taken to be R_1=25h and γ=15°. The values of non-linear critical temperature differences of alumina, aluminum, FGM-A and FGM-B truncated conical shells within CST and SDT decrease, as the ratio, L/R_1 increases. As the L/R_1 increases from 0.2 to 0.5, the influences of transverse shear stresses on the non-linear critical temperature differences of FGM-A truncated conical shells gradually decrease, from 7.98% to 0.7%, from 7.8% to 0.81%, from 8.75% to 0.81% and from 7.79% to 0.81% for k=0.5; 1.0; 2.0; 10, respectively. The influences of FGM A and FGM B profiles on the non-linear critical temperature differences are changed by certain values of k with the increasing of L/R_1. Comparing FGM A and FGM-B conical shells with an alumina conical shell, the influences of FGM-A and FGM-B profiles on the values of non-linear critical temperature differences of truncated conical shells within SDT decrease, while comparing they with an aluminum conical shell, these influences increase, as the ratio L/R_1 increases from 0.2 to 0.5 for k=0.5; 1.0; 2.0; 10. Comparing FGM-A and FGM-B conical shells with the alumina conical shell, the influence of FGM-A profiles on the T_{NLcr}^{SDT} is lower than the influence of FGM-B profiles for k<2, while those higher for k>2.

The distribution of the values of T_{NLcr}^{SDT} and T_{NLcr}^{CST} (in C°) for alumina, aluminum, FGM-A and FGM-B truncated conical shells depending on the R_1/h are plotted in Figs. 4 and 5. The volume fraction index and truncated conical shells characteristics are taken to be k=0.5; 1.0; 2.0; 10, and R_1=5L andγ=15°. The magnitudes of non-linear critical temperature differences of alumina, aluminum, FGM-A and FGM-B truncated conical shells based on the SDT and CST decrease with the increasing of the ratio, R_1/h. The magnitudes of T_{NLcr}^{SDT} for FGM-A conical shells lower than those of FGM-B conical shells, for all ratio, R_1/h. Figs. 4 and 5 reveals that with the increasing of R_1 from 20h to 50h, the effects of shear stresses on the magnitudes of non-linear critical temperature differences of FGM-A truncated conical shells decrease; from 12.37% to 1.57%, from 12.12% to 1.52%, from 13.52% to 1.74% and from 12.12% to 1.52%, while these effects for FGM-B truncated conical shells decrease; from 13.54% to 1.73%, from 12.11% to 1.52%, from 11.28% to 1.38% and from 12.14% to 1.54%, for k=0.5; 1.0; 2.0; 10, respectively. Comparing the non-linear critical temperature differences of FGM-A and FGM-B truncated conical shells with the alumina conical shell, the effects of FGM-A and FGM-B profiles on the non-linear critical temperature differences slightly decrease with the increasing of the ratio, R_1/h for k=0.5; 1.0; 2.0; 10. Comparing the non-linear critical temperature differences of FGM-A and FGM-B truncated conical shells with the aluminum conical shell, the effects of FGM-A profiles increase for k=0.5; 1.0; 2.0; 10, whereas, the effects of FGM-B profiles on the T_{NLcr}^{SDT} decrease significantly for k=1.0; 2.0, this effect varies for k=0.5 and it increases for k= 10 with the increasing of the ratio, R_1/h.

6. Concluding remarks

In this study, the thermoelastic buckling of FGM conical shells under non-linear temperature rise across the thickness in the framework of the SDT is investigated. To the derivation of the basic

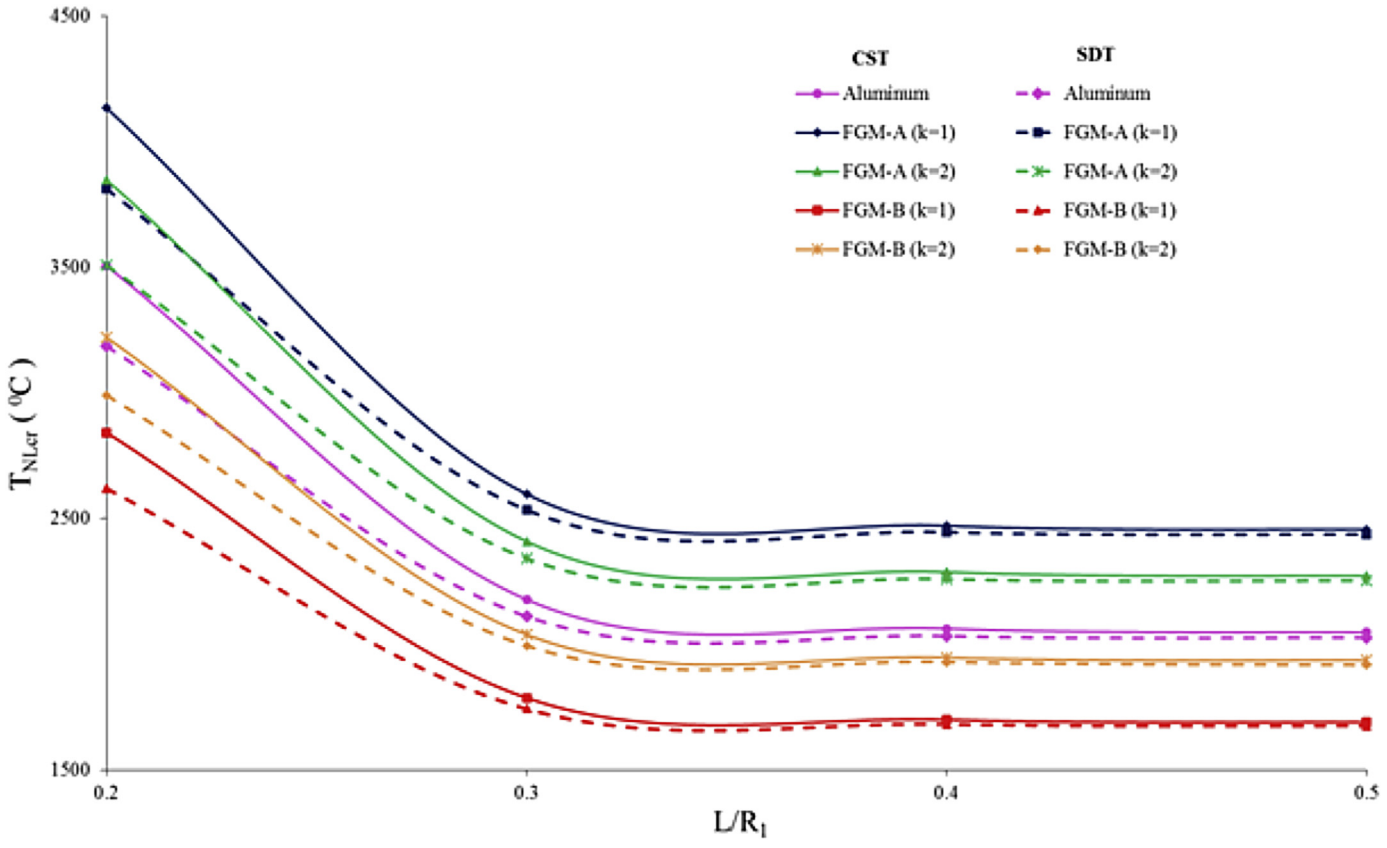

Fig. 2. The distribution of the values of T_{NLcr}^{SDT} and T_{NLcr}^{CST} for aluminum, FGM-A and FGM-B truncated conical shells versus the L/R_1 with k=1 and 2.

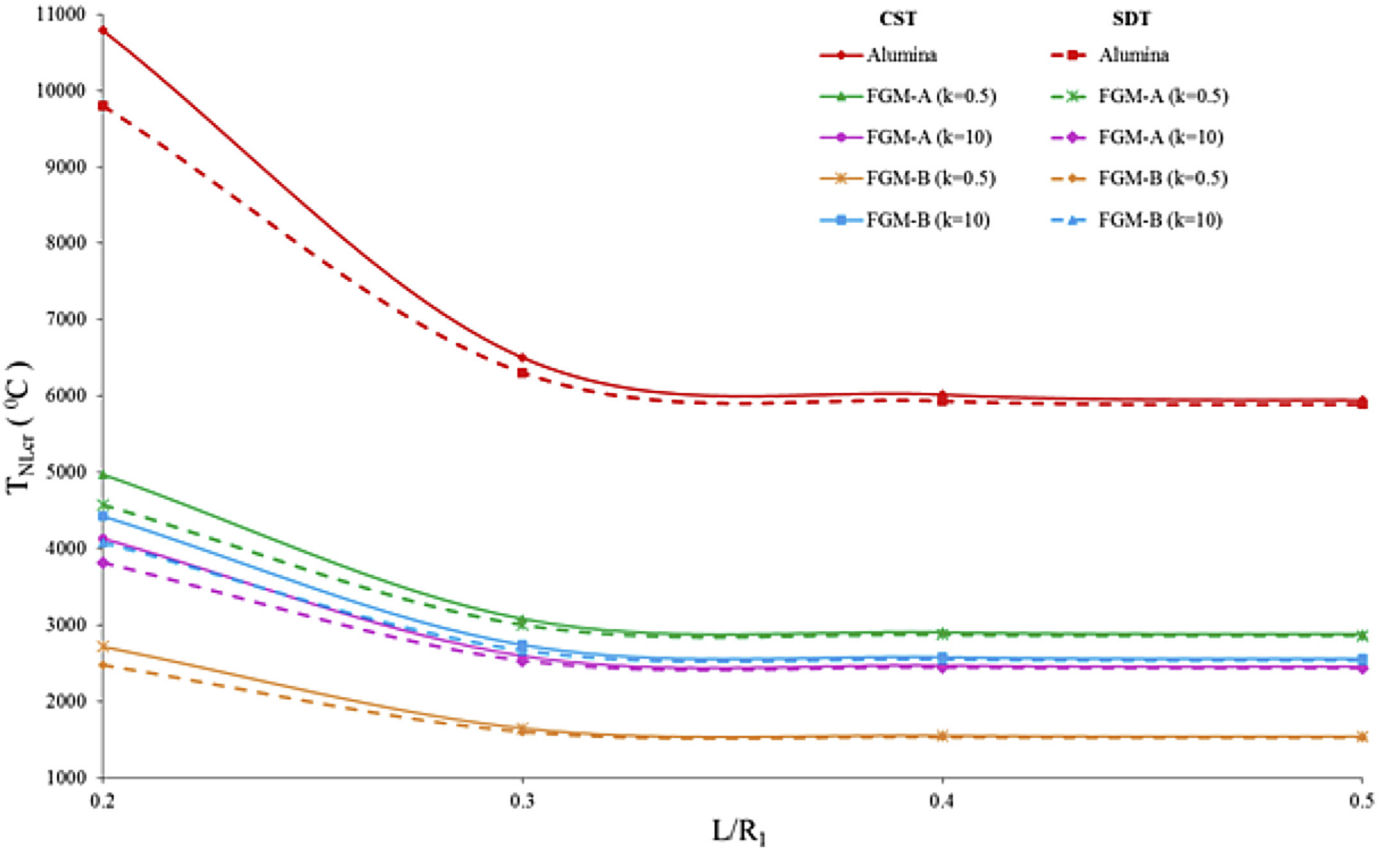

Fig. 3. The distribution of the values of T_{NLcr}^{SDT} and T_{NLcr}^{CST} for alumina, FGM-A and FGM-B truncated conical shells versus the L/R_1 with k=0.5 and 10.

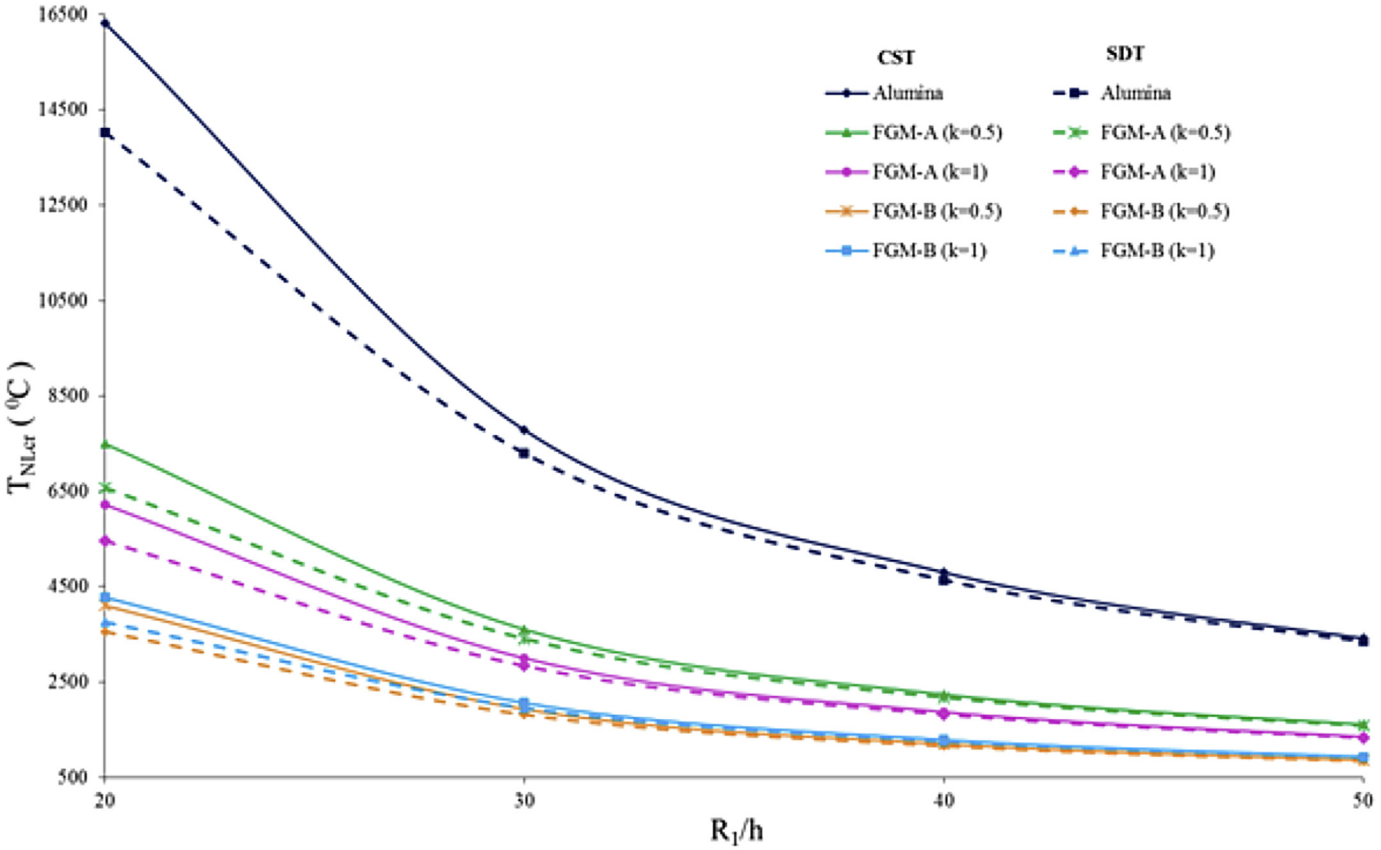

Fig. 4. The distribution of the values of T_{NLcr}^{SDT} and T_{NLcr}^{CST} for alumina, FGM-A and FGM-B truncated conical shells versus the R_1/h with k=0.5 and 1.0.

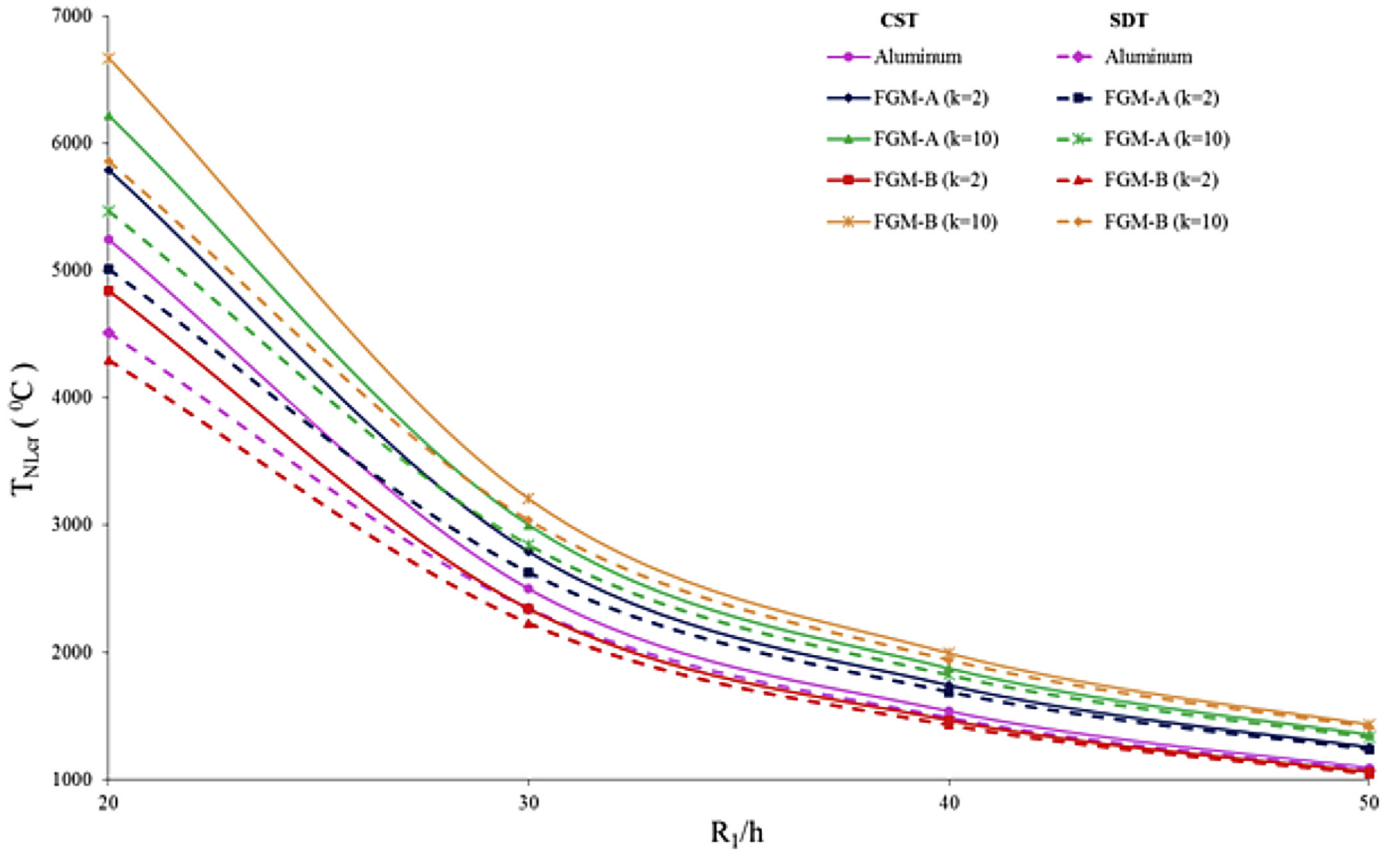

Fig. 5. The distribution of the values of T_{NLcr}^{SDT} and T_{NLcr}^{CST} for aluminum, FGM-A and FGM-B truncated conical shells versus the R_1/h with $k = 2$ and 10.

equations of FGM truncated conical shells under non-linear thermal loadings in the framework of the SDT is used modified Donnell-type shell theory. The Galerkin method is used to obtain the formula for non-linear buckling temperature difference of freely supported FGM truncated conical shell in the framework of the SDT. By changing the properties of FGMs and volume fraction index, the effect of transverse shear deformations on the non-linear buckling temperature difference is evaluated by comparing with the results of the CST. Meanwhile, the effect of geometric parameters on the non-linear buckling temperature difference of the shear deformable FGM conical shells is discussed in detail.

Appendix A

In Eq. (20), the details of differential operators $L_{ij}(1, 2, \ldots, 4)$ are described by

$$L_{11}(\Psi) = \frac{a_2 h}{S_2^4 e^{4x}}\left(\frac{\partial^4}{\partial x^4} - 5\frac{\partial^3}{\partial x^3} + 6\frac{\partial^2}{\partial x^2} + 3\frac{\partial^2}{\partial \varphi^2} - \frac{\partial^3}{\partial x \partial \varphi^2}\right) + \frac{(a_1 - a_5)h}{S_2^4 e^{4x}}\left(\frac{\partial^4}{\partial x^2 \partial \varphi^2} - 4\frac{\partial^3}{\partial x \partial \varphi^2} + 3\frac{\partial^2}{\partial \varphi^2}\right)$$

$$L_{12}(w) = -\frac{a_3}{S_2^4 e^{4x}}\left(\frac{\partial^4}{\partial x^4} - \frac{\partial^3}{\partial x \partial \varphi^2} - 5\frac{\partial^3}{\partial x^3} + 6\frac{\partial^2}{\partial x^2} + 3\frac{\partial^2}{\partial \varphi^2}\right) - \frac{a_4 + a_6}{S_2^4 e^{4x}}\left(\frac{\partial^4}{\partial x^2 \partial \varphi^2} - 4\frac{\partial^3}{\partial x \partial \varphi^2} + 3\frac{\partial^2}{\partial \varphi^2}\right)$$

$$L_{13}(\eta_1) = \frac{a_{11}}{S_2^3 e^{3x}}\frac{\partial^3}{\partial x \partial \varphi^2} + \frac{a_7}{S_2^3 e^{3x}}\frac{\partial^3}{\partial x^3} - \frac{2a_7 + a_9}{S_2^3 e^{3x}}\frac{\partial^2}{\partial x^2} + \frac{2a_9}{S_2^3 e^{3x}}\frac{\partial}{\partial x} - \frac{J}{S_2 e^x}\frac{\partial}{\partial x} - \frac{a_{11}}{S_2^3 e^{3x}}\frac{\partial^2}{\partial \varphi^2}$$

$$L_{14}(\eta_2) = \frac{a_{12} + a_8}{S_2^3 e^{3x}}\frac{\partial^3}{\partial x^2 \partial \varphi} - \frac{a_{10} + 2a_8 + 2a_{12}}{S_2^3 e^{3x}}\frac{\partial^2}{\partial x \partial \varphi} + \frac{2a_{10}}{S_2^3 e^{3x}}\frac{\partial}{\partial \varphi}$$

$$L_{21}(\Psi) = \frac{a_2 h}{S_2^3 e^{3x}}\left(\frac{\partial^4}{\partial \varphi^4} + \frac{\partial^3}{\partial x \partial \varphi^2}\right) + \frac{(a_1 - a_5)h}{S_2^3 e^{3x}}\left(\frac{\partial^4}{\partial x^2 \partial \varphi^2} - \frac{\partial^3}{\partial x \partial \varphi^2}\right)$$

$$L_{22}(w) = -\frac{a_6 + a_4}{S_2^3 e^{3x}}\left(\frac{\partial^4}{\partial x^2 \partial \varphi^2} - \frac{\partial^3}{\partial x \partial \varphi^2}\right) - \frac{a_3}{S_2^3 e^{3x}}\left(\frac{\partial^4}{\partial \varphi^4} + \frac{\partial^3}{\partial x \partial \varphi^2}\right)$$

$$L_{23}(\eta_1) = \frac{a_9 + a_{11}}{S_2^3 e^{3x}}\frac{\partial^3}{\partial x \partial \varphi^2} + \frac{a_{11}}{S_2^2 e^{2x}}\frac{\partial^2}{\partial \varphi^2}$$

$$L_{24}(\eta_2) = \frac{a_{12}}{S_2^2 e^{2x}}\frac{\partial^3}{\partial x^2 \partial \varphi} + \frac{a_{12}}{S_2^2 e^{2x}}\frac{\partial^2}{\partial x \partial \varphi} + \frac{a_{10}}{S_2^2 e^{2x}}\frac{\partial^3}{\partial \varphi^3} - J\frac{\partial}{\partial \varphi}$$

$$L_{31}(\Psi)=\frac{b_1 h}{S_2^4 e^{4x}}\left(\frac{\partial^4}{\partial\varphi^4}+\frac{\partial^4}{\partial x^4}-4\frac{\partial^3}{\partial x^3}+4\frac{\partial^2}{\partial x^2}+2\frac{\partial^2}{\partial\varphi^2}\right)+\frac{(b_5+2b_2)h}{S_2^4 e^{4x}}\left(\frac{\partial^4}{\partial x^2\partial\varphi^2}-2\frac{\partial^3}{\partial x\partial\varphi^2}\frac{\partial^2}{\partial\varphi^2}\right)$$

$$L_{32}(w)=\frac{\cot\gamma}{S_2^3 e^{3x}}\left(\frac{\partial^2}{\partial x^2}-\frac{\partial}{\partial x}\right)+\frac{b_6-2b_3}{S_2^4 e^{4x}}\left(\frac{\partial^4}{\partial x^2\partial\varphi^2}-2\frac{\partial^3}{\partial x\partial\varphi^2}+\frac{\partial^2}{\partial\varphi^2}\right)$$
$$-\frac{b_4}{S_2^4 e^{4x}}\left(\frac{\partial^4}{\partial x^4}-4\frac{\partial^3}{\partial x^3}+4\frac{\partial^2}{\partial x^2}+\frac{\partial^4}{\partial\varphi^4}+2\frac{\partial^2}{\partial\varphi^2}\right)$$

$$L_{33}(\eta_1)=\frac{b_{11}+b_7}{S_2^3 e^{3x}}\frac{\partial^3}{\partial x\partial\varphi^2}+\frac{b_9}{S_2^3 e^{3x}}\frac{\partial^3}{\partial x^3}-\frac{b_9+b_7}{S_2^3 e^{3x}}\frac{\partial^2}{\partial x^2}+\frac{b_7}{S_2^3 e^{3x}}\frac{\partial}{\partial x}$$

$$L_{34}(\eta_2)=\frac{b_8}{S_2^3 e^{3x}}\frac{\partial^3}{\partial\varphi^3}+\frac{b_{12}+b_{10}}{S_2^3 e^{3x}}\frac{\partial^3}{\partial x^2\partial\varphi}-\frac{b_{10}+b_8}{S_2^3 e^{3x}}\frac{\partial^2}{\partial x\partial\varphi}+\frac{b_8}{S_2^3 e^{3x}}\frac{\partial}{\partial\varphi}$$

$$L_{41}(\Psi)=\frac{\cot\gamma}{S_2^3 e^{3x}}\left(\frac{\partial^2}{\partial x^2}-\frac{\partial}{\partial x}\right),\quad L_{42}(w)=-\Phi\left(\frac{\partial^2}{\partial x^2}-\frac{\partial}{\partial x}\right),$$
$$L_{43}(\eta_1)=\frac{J}{S_2 e^x}\left(\frac{\partial}{\partial x}+1\right),\quad L_{44}(\eta_2)=\frac{J}{S_2 e^x}\frac{\partial}{\partial\varphi}\tag{A1}$$

where the following definitions apply:

Appendix B

In Eq. (23), $p_{ij}(i, j=1, 2, \ldots, 4)$ are expressed as

$$a_1=d_1^1b_1+d_2^1b_2,\quad a_2=d_1^1b_2+d_2^1b_1,\quad a_3=d_1^1b_3+d_2^1b_4+d_1^2,\quad a_4=d_1^1b_4+d_2^1b_3+d_2^2,$$
$$a_5=d_6^1b_5,\quad a_6=d_6^1b_6+2d_6^2,\quad a_7=d_1^1b_7+d_2^1b_9+d_7^1,\quad a_8=d_1^1b_8+d_2^1b_{10}+d_8^1,$$
$$a_9=d_2^1b_7+d_1^1b_9+d_9^1,\quad a_{10}=d_2^1b_8+d_1^1b_{10}+d_{10}^1,\quad a_{11}=d_{11}^1-d_6^1b_{11},\quad a_{12}=d_{12}^1-d_6^1b_{12},$$
$$b_1=\frac{d_1^0}{d_0},\quad b_2=-\frac{d_2^0}{d_0},\quad b_3=\frac{d_2^0d_2^1-d_1^1d_1^0}{d_0},\quad b_4=\frac{d_2^0d_1^1-d_2^1d_1^0}{d_0},\quad b_5=\frac{1}{d_6^0},\quad b_6=-\frac{2d_6^1}{d_6^0},\tag{A2}$$
$$b_7=\frac{d_9^0d_2^0-d_{15}^0d_1^0}{d_0},\quad b_8=\frac{d_{10}^0d_2^0-d_8^0d_1^0}{d_0},\quad b_9=\frac{d_7^0d_2^0-d_9^0d_1^0}{d_0},\quad b_{10}=\frac{d_7^0d_2^0-d_{10}^0d_1^0}{d_0},$$
$$b_{11}=\frac{d_{11}^0}{d_6^0},\quad b_{12}=\frac{d_{12}^0}{d_6^0},\quad d_0=\left(d_1^0\right)^2-\left(d_2^0\right)^2,\quad J=2\sinh(h/2)-h\cosh(1/2).$$

in which $d_j^{k_1}(j=1,2,6)$ and $d_j^{k_2}(j=7,8,\ldots12)$ are described by

$$d_1^{k_1}=\int_{-h/2}^{h/2}z^{k_1}K_{11}(Z)dz,\ d_2^{k_1}=\int_{-h/2}^{h/2}z^{k_1}K_{12}(Z)dz,\ d_6^{k_1}$$
$$=\int_{-h/2}^{h/2}z^{k_1}K_{33}(Z)dz\quad k_1=0,1,2;$$
$$d_7^{k_2}=\int_{-h/2}^{h/2}z^{k_2}I(z)K_{11}(Z)\mathrm{d}z,\quad d_8^{k_2}=\int_{-h/2}^{h/2}z^{k_2}I(z)K_{12}(Z)\mathrm{d}z,$$
$$d_9^{k_2}=\int_{-h/2}^{h/2}z^{k_2}I(z)K_{12}(Z)\mathrm{d}z,\quad d_{10}^{k_2}=\int_{-h/2}^{h/2}z^{k_2}I(z)K_{11}(Z)\mathrm{d}z,$$
$$d_{11}^{k_2}=\int_{-h/2}^{h/2}z^{k_2}I(z)K_{33}(Z)\mathrm{d}z,\quad d_{12}^{k_2}=\int_{-h/2}^{h/2}z^{k_2}I(z)K_{33}(Z)\mathrm{d}z,$$
$$k_2=0,1.\tag{A3}$$

$$p_{11}=-2h\chi_{-1}\left\{a_2\left[3(\lambda-1)(\lambda+1)^3+2\alpha^2(\lambda+4)(\lambda+1)-\alpha^4\right]\right.$$
$$\left.+(a_5-a_1)\beta^2\left(\lambda^2-\lambda-2+\alpha^2\right)\right\}-h\chi_{-1}\left\{6(a_5-a_1)\beta^2+a_2\right.$$
$$\left.\times\left[3\beta^2-5(\lambda+1)^2(4\lambda-5)-\alpha^2(20\lambda+23)+12\left(\lambda^2-\lambda-2\right)\right]\right\},$$
$$p_{12}=\frac{2\chi_{-2}}{S_2}\left\{(a_4+a_6)\beta^2\left[\lambda(\lambda-2)+\alpha^2+4\beta^2-3\right]+a_3\left(14\lambda^3+6\lambda\alpha^2\right.\right.$$
$$\left.\left.-21\lambda^2+4\alpha^2-3\lambda^4-2\lambda^2\alpha^2+\alpha^4+12\lambda-2\beta^2\right)\right\},$$
$$p_{13}=\frac{\chi_{-1}}{\alpha}\left\{a_{11}\left[(2\lambda-1)\lambda+2\alpha^2\right]\beta^2-a_7\left[(2\lambda-1)\lambda^3+3\lambda\alpha^2-2\alpha^4\right]\right.$$
$$\left.+\left(\alpha^2-\lambda^2+2\lambda^3+2\lambda\alpha^2\right)\times(2a_7+a_9)-2a_9\left[(2\lambda-1)\lambda+2\alpha^2\right]\right\}$$
$$-\frac{\chi_1}{\alpha}\left\{-I_3\left[\lambda(1+2\lambda)+2\alpha^2\right]S_2^2+a_{11}(2\lambda+1)\beta^2\right\},$$
$$p_{14}=\beta\chi_{-1}\left\{3a_{10}-2(a_{12}+a_8)\left[(\lambda-1)\lambda+\alpha^2+1\right]\right\},$$

$$p_{21}=2h\beta^2\chi_0\left[a_2\left(\beta^2-1\right)+(a_1-a_5)\left(\lambda^2+\alpha^2\right)\right],$$

$$p_{22}=\frac{\beta^2\chi_{-1}}{S_2}\left\{a_3\left(1-2\beta^2\right)-2(a_6+a_4)\left[(\lambda-1)\lambda+\alpha^2+0.5\right]\right\},$$

$$p_{23}=\frac{\beta^2}{\alpha}\left\{\frac{(a_9+a_{11})\left[(2\lambda-1)\lambda+2\alpha^2\right]\chi_{-1}}{\alpha S_2}+2a_{11}\chi_0\lambda\right\},$$

$$p_{24}=-2\beta\left\{\left[a_{12}\left(\alpha^2+\lambda^2\right)+a_{10}\beta^2\right]\chi_0+I_4\chi_2S_2^2\right\},$$

$$\begin{aligned}p_{31}=&2h\chi_0\left\{(b_5+2b_2)\beta^2\left(\lambda^2+\alpha^2\right)+b_1\left[\beta^2\left(\beta^2-2\right)+\alpha^4\right.\right.\\&\left.\left.-(\lambda+1)^3(3\lambda-1)-2(\lambda+3)(\lambda+1)\alpha^2+8(\lambda+1)\left(\alpha^2+\lambda^2\right)\right]\right\},\\p_{32}=&-\frac{2\chi_{-1}}{S_2}\left[(2b_3-b_6)\left(\lambda^2-\lambda+\alpha^2\right)+b_4\left(10\lambda^3-3\lambda^4-2\alpha^2\lambda^2\right.\right.\\&\left.\left.+\alpha^4+\beta^4-10\lambda^2+6\alpha^2\lambda-2\alpha^2-2\beta^2+4\lambda\right)\right]\\&-2\chi_0\left(\lambda^2+\alpha^2\right)\cot\gamma,\\p_{33}=&\frac{2\chi_0\left(\alpha^2+\lambda^2\right)}{\alpha}\left[(b_{11}+b_7)\beta^2-b_9\left(\lambda^2-\alpha^2\right)+(b_9+b_7)\lambda-b_7\right],\\p_{34}=&2\chi_0\beta\left[b_8\left(1-\beta^2\right)-(b_{12}+b_{10})\left(\alpha^2+\lambda^2\right)\right],\end{aligned}$$

$$\begin{aligned}p_{41}=&-\frac{2\chi_0h\left(\alpha^2+\lambda^2\right)\cot\gamma}{S_2^2},\\p_{43}=&-\frac{\chi_1I_3\left[(2\lambda+1)(\lambda+1)+2\alpha^2\right]}{S_2\alpha},\quad p_{44}=\frac{2I_4\chi_1\beta}{S_2},\\p_T=&-\frac{2\left(\alpha^2+\lambda^2\right)\chi_0}{S_2^2}\end{aligned}\tag{B1}$$

where

$$\chi_i=\frac{\alpha^2\left[1-e^{-2(\lambda+i/2)\chi_0}\right]}{8\left[(\lambda+i/2)^2+\alpha^2\right](\lambda+i/2)};\quad i=-2;\ -1;\ 0;\ 1;\ 2.\tag{B2}$$

Appendix C

In Eq. (27), $\bar{u}_j(j=1,2,3)$ and $\bar{p}_T$ are given by

$$\begin{aligned}\bar{u}_1=&\left\{a_2\left(u_{01}-4u_{02}+4u_{03}+2\beta^4-4\beta^2\right)\chi_{-1}+(2a_1-a_5)\beta^2\right.\\&\times(4-u_{03})\chi_{-1}\ -2\left[(\lambda-1)(\lambda+1)+\alpha^2+1\right]\chi_0S_2\cot\gamma\Big\}\\&\times\left[b_4\left(4t_7-2\beta^4+4\beta^2-t_6-4t_5\right)\chi_{-1}\ -(b_6-2b_3)\beta^2\right.\\&\left.\times(t_5+2)\chi_{-1}-2\left(\lambda^2+\alpha^2\right)\chi_0S_2\cot\gamma\right],\\\bar{u}_2=&\left[a_3\left(2\beta^4-4\beta^2+u_{05}-4u_{06}+4u_{07}\right)+(2a_4+a_6)\beta^2\right.\\&\left.\times(6-u_{04})\right]\chi_{-2}\ \times\left[b_1\left(2\beta^4-4\beta^2+t_2-4t_3+4t_1\right)\right.\\&\left.-(2b_2+b_5)\beta^2(t_1+2)\right]\chi_0,\\\bar{u}_3=&\left[b_1\left(2\beta^4-4\beta^2+t_2-4t_3+4t_1\right)-(2b_2+b_5)\beta^2(t_1+2)\right]\chi_0,\\\bar{p}_T=&2\left(\lambda^2+\alpha^2\right)S_2^2\chi_0,\end{aligned}\tag{C1}$$

where the following definitions apply:

$$\begin{aligned}u_{01}=&-2\left[3(\lambda+1)^3(\lambda-1)-6\alpha^2(\lambda+1)\lambda-\alpha^4\right],\\u_{02}=&-\left[\alpha^2(4\lambda+7)+(\lambda+1)^2(4\lambda-5)\right],\\u_{03}=&-2\left[(\lambda-2)(\lambda+1)+\alpha^2\right],\quad u_{04}=-2\left[(\lambda-2)\lambda+\alpha^2\right],\\u_{05}=&-2\left[\lambda^3(3\lambda-4)-2\alpha^2\lambda(3\lambda-2)-\alpha^4\right],\\u_{06}=&-2\left[\alpha^2(2\lambda+1)+\lambda^2(2\lambda-3)\right],\\u_{07}=&-2\left[(\lambda-2)\lambda+\alpha^2\right],\\t_1=&-2\left[(\lambda-1)(\lambda+1)+\alpha^2\right],\\t_2=&-2\left[(\lambda+1)^3(3\lambda-1)+2\alpha^2(\lambda+1)(\lambda+3)-\alpha^4\right],\\t_3=&-\left[\alpha^2(4\lambda+6)+(\lambda+1)^2(4\lambda-2)\right],\\t_4=&-2\left[(\lambda-1)(\lambda+1)+\alpha^2\right],\quad t_5=-2\left[(\lambda-1)\lambda+\alpha^2\right],\\t_6=&-2\left[\lambda^3(3\lambda-2)+2m_1^2(\lambda+1)\lambda-\alpha^4\right],\\t_7=&-\left[\alpha^2(4\lambda+1)+\lambda^2(4\lambda-3)\right].\end{aligned}\tag{C2}$$

References

[1] Koizumi M. FGM activities in Japan. Compos B Eng 1997;28:1–4.
[2] Suresh S, Mortensen A. Fundamentals of functionally graded materials. London: IOM Communications Ltd; 1998.
[3] Miyamoto Y, Kaysser WA, Rabin BH, Kawasaki A, Ford RG. Functionally graded materials: design, processing and applications. Dordrecht. Kluwer Academic Publishers.; 1999.
[4] Pindera MJ, Arnold SM, Aboudi J, Hui D. Use of composites in functionally graded materials. Compos Eng 1994;4:7–9.
[5] Zheng LY, Lau KT, Zhao Li-X, Zhang YQ, Hui D. Mechanical and thermal properties of Nano-Al_2O_3/Nylon 6 composites. Chemil Eng Commun 2010;197:343–51.
[6] Shahsiah R, Eslami MR. Functionally graded cylindrical shell thermal instability based on improved Donnell equations. AIAA J 2003;41:1819–26.
[7] Na KS, Kim JH. Three-dimensional thermal buckling analysis of functionally graded materials. Compos B Eng 2004;35:429–37.
[8] Wu L, Jiang Z, Liu J. Thermoelastic stability of functionally graded cylindrical shells. Compos Struct 2005;70:60–8.
[9] Shariyat M. Dynamic thermal buckling of suddenly heated temperature-dependent FGM cylindrical shells, under combined axial compression and external pressure. Int J Solid Struct 2008;45:2598–612.
[10] Cavalcante MAA, Marques SPC, Pindera MJ. Transient finite-volume analysis of a graded cylindrical shell under thermal shock loading. Mech Adv Mater Struct 2011;18:53–67.
[11] Wosu SN, Hui D, Daniel L. Hygrothermal effects on the dynamic compressive properties of graphite/epoxy composite material. Compos B Eng 2012;43:841–55.
[12] Heydarpour Y, Malekzadeh P, Golbahar HMR, Vaghefi M. Thermoelastic analysis of rotating laminated functionally graded cylindrical shells using layerwise differential quadrature method. Acta Mech 2012;223:81–93.
[13] Bagherizadeh E, Kiani Y, Eslami MR. Thermal buckling of functionally graded material cylindrical shells on elastic foundation. AIAA J 2012;50:500–3.
[14] Shen HS. Thermal buckling and postbuckling behavior of functionally graded carbon nanotube-reinforced composite cylindrical shells. Compos B Eng 2012;43:1030–8.
[15] Shariyat M, Asgari D. Nonlinear thermal buckling and postbuckling analyses of imperfect variable thickness temperature-dependent bidirectional functionally graded cylindrical shells. Int J Pres Ves Pip 2013;111–112:310–20.
[16] Sheng GG, Wang X. An analytical study of the non-linear vibrations of functionally graded cylindrical shells subjected to thermal and axial loads. Compo Struct 2013;97:261–8.
[17] Dai HL, Qi LL, Zheng HY. Buckling analysis for a ring-stiffened FGM cylindrical shell under hydrostatic pressure and thermal loads. J Mech 2014;30:403–10.
[18] Mansouri MH, Shariyat M. Biaxial thermo-mechanical buckling of orthotropic auxetic FGM plates with temperature and moisture dependent material properties on elastic foundations. Compos B Eng 2015;83:88–104.
[19] Sun J, Xu X, Lim CW, Qiao W. Accurate buckling analysis for shear deformable FGM cylindrical shells under axial compression and thermal loads. Compos Struct 2015;123:246–56.
[20] Sun J, Xu X, Lim CW, Zhou Z, Xiao S. Accurate thermo-electro-mechanical buckling of shear deformable piezoelectric fiber-reinforced composite cylindrical shells. Compos Struct 2016;141:221–31.

[21] Alibeigloo A. Thermoelastic analysis of functionally graded carbon nanotube reinforced composite cylindrical panel embedded in piezoelectric sensor and actuator layers. Compos Part B Eng 2016;98:225–43.
[22] Jabbari M, Meshkini M, Eslami MR. Mechanical and thermal stresses in FGPPM hollow cylinder due to radially symmetric loads. J Pres Ves Techn ASME 2016;138. 011207.
[23] Khazaeinejad P, Usmani AS. On thermo-mechanical nonlinear behaviour of shallow shells. Int J Non-Lin Mech 2016;82:114–23.
[24] Bhangale RK, Ganesan RK, Padmanabhan C. Linear thermo–elastic buckling and free vibration behavior of FG truncated conical shell. J Sound Vib 2006;292:341–71.
[25] Sofiyev AH. Thermo-elastic stability of functionally graded truncated conical shells. Compos Struct 2007;77:56–65.
[26] Naj R, Boroujerdy SM, Eslami MR. Thermal and mechanical instability of functionally graded truncated conical shells. Thin-Walled Struct 2008;46:65–78.
[27] Torabi J, Kiani Y, Eslami MR. Linear thermal buckling analysis of truncated hybrid FGM conical shells. Compos B Eng 2013;50:265–72.
[28] Akbari M, Kiani Y, Eslami MR. Thermal buckling of temperature-dependent FGM conical shells with arbitrary edge supports. Acta Mech 2015;226:897–915.
[29] Mirzaei M, Kiani Y. Thermal buckling of temperature dependent FG-CNT reinforced composite conical shells. Aerosp Sci Techn 2015;47:42–53.
[30] Duc ND, Pham HC. Nonlinear thermal stability of eccentrically stiffened functionally graded truncated conical shells surrounded on elastic foundations. Euro J Mech- A/Solids 2015;50:120–31.
[31] Ferreira AJM, Roque CMC, Neves AMA, Jorge RMN, Soares CMM, Reddy JN. Buckling analysis of isotropic and laminated plates by radial basis functions according to a higher-order shear deformation theory. Thin-Walled Struct 2011;49:804–11.
[32] Viola E, Rossetti L, Fantuzzi N, Tornabene F. Static analysis of functionally graded conical shells and panels using the generalized unconstrained third order theory coupled with the stress recovery. Compos Struct 2014;112:44–65.
[33] Mansouri MH, Shariyat M. Thermal buckling predictions of three types of high-order theories for the heterogeneous orthotropic plates, using the new version of DQM. Compos Struct 2014;113:40–55.
[34] Liu B, Ferreira AJM, Xing YF, Neves AMA. Analysis of functionally graded sandwich and laminated shells using a layerwise theory and a differential quadrature finite element method. Compos Struct 2016;136:546–53.
[35] Tornabene F, Fantuzzi N, Viola E, Batra RC. Stress and strain recovery for functionally graded free-form and doubly-curved sandwich shells using higher-order equivalent single layer theory. Compos Struct 2015;119:67–89.
[36] Tornabene F, Fantuzzi N, Bacciocchi M, Viola E. Effect of agglomeration on the natural frequencies of functionally graded carbon nanotube-reinforced laminated composite doubly-curved shells. Compos B Eng 2016;89:187–218.
[37] Sofiyev AH. Thermoelastic stability of freely supported functionally graded conical shells within the shear deformation theory. Compos Struct 2016;152:74–84.
[38] Reddy JN. Analysis of functionally graded plates. Int J Numer Meth Engng 2000;47:663–84.
[39] Shen HS. Functionally graded materials. In: nonlinear analysis of plates and shells. s: CRC Press; 2009.
[40] Ambartsumyan SA. Theory of anisotropic shells. NASA; 1964. TT F-118.
[41] Timarci T, Soldatos KP. Comparative dynamic studies for symmetrical cross-ply circular cylindrical-shells on the basis of a unified shear-deformable shell theory. J Sound Vib 1995;187:609–24.
[42] Lu SY, Chang LK. Thermal buckling of conical shells. AIAA J 1957;5(10):1877–82.